Reverse intersystem crossing of single deuterated perylene molecules in a dibenzothiophene matrix

Smit, R.; Ristanovic, Z.; Kozankiewicz, B.; Orrit, M.A.G.J.

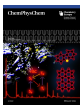

Reverse Intersystem Crossing of Single Deuterated Perylene Molecules in a Dibenzothiophene Matrix

Robert Smit,[a] Zoran Ristanović,[a] Bolesław Kozankiewicz,[b] and Michel Orrit*[a]

Intersystem crossing to the long-lived metastable triplet state is often a strong limitation on fluorescence brightness of single molecules, particularly for perylene in various matrices. In this paper, we report on a strong excitation-induced reverse intersystem crossing (rISC), a process where single perylene molecules in a dibenzothiophene matrix recover faster from the triplet state, turning into bright emitters at saturated excitation powers. With a detailed study of single-molecule fluorescence autocorrelations, we quantify the effect of rISC. The intrinsic lifetimes found for the two effective triplet states (8.5 ± 0.4 ms and 64 ± 12 ms) become significantly shorter, into the sub-millisecond range, as the excitation power increases and fluorescence brightness is ultimately enhanced at least fourfold. Our results are relevant for the understanding of triplet state manipulation of single-molecule quantum emitters and for markedly improving their brightness.

1. Introduction

Triplet states are usually a bottleneck for single-molecule fluorescence spectroscopy (SMS) at cryogenic temperatures. As the single molecule enters the triplet state, its fluorescence is cut off for the time that it remains in this metastable dark state.[1] For some fluorophores, such as perylene, this time is relatively long – in the range of milliseconds.[2] The result is a relatively poor brightness of single perylene molecules and this is the main reason that their study in SMS has been mostly overtaken by bright and stable emitters such as dibenzoterrylene, known to have a very low triplet yield and a triplet lifetime on the order of tens of microseconds.[3,4] Nevertheless, the fluorescence intermittency originating from the existence of triplet dark states can be exploited in cryogenic super-resolution localization schemes based on stochastic blinking of single emitters.[5–9] One of the applications of single molecules as bright emitters is as very sensitive probes of their local environment by means of perturbations on their optical transitions. The ideal case of an uninterrupted stream of photons, caused by a very low triplet yield and/or a very short triplet lifetime, would act as a stable information source for probing local effects. Some of these proven concepts of single molecules as probes are high sensitivity to electric fields and charges by an electrically- or optically-induced Stark effect,[10–12] or single molecules as nano-microphones of mechanically induced strain.[13] Recently, single-molecule emitters have also received significant attention as stable and tunable single-photon sources and non-linear elements in integrated photonic devices.[14–18]

However, single molecules are not only studied for their emissive properties originating from the singlet transition. Unlike the singlet, the triplet state has a non-zero spin and therefore makes experiments involving static and variable magnetic fields possible. Such are the optically detected magnetic resonance (ODMR) experiments on pentacene in p-terphenyl, which showed that the transitions between triplet sublevels can be induced by microwaves that match the (zero-field) splitting in energy.[19] However, one has to rely on the stochastic nature of ISC transitions to the triplet state before the spin state can be manipulated. Optical control of the switching between a single molecule's singlet ground state and triplet excited state remains to be demonstrated.[20] Perylene, an interesting candidate for such an experiment, has both its singlet and triplet transitions conveniently placed in wavelength ranges accessible by the well-established Ti:sapphire laser, directly for the triplet transition, and through the second harmonic of another Ti:sapphire laser in the blue region[21] for the singlet. However, for a direct optical excitation of the molecule to the triplet state, the corresponding wavelength of the $S_0 \rightarrow T_1$ transition needs to be found first. So far, the 0–0 zero-phonon line (ZPL) for the phosphorescence of perylene-doped matrices has been detected solely for perylene in anthracene[22] and was determined to be around $12844 \pm 1\ \mathrm{cm}^{-1}$, blue-shifted by $472\ \mathrm{cm}^{-1}$ compared to the origin of phosphorescence found for a pure perylene crystal.[23] Unfortunately, fluorescence from single perylene molecules in anthracene could not be detected, probably because of intermolecular ISC.[24] For future studies on the phosphorescence of perylene in the dibenzothiophene matrix, we chose to study deuterated perylene in this work, instead of the commonly employed hydrogenated perylene. For the deuterated analogue of perylene, it is expected that non-radiative

[a] R. Smit, Dr. Z. Ristanović, Prof. M. Orrit
Huygens-Kamerlingh Onnes Laboratory, LION
Postbus 9504, 2300 RA, Leiden, The Netherlands
E-mail: Orrit@Physics.LeidenUniv.nl
[b] Prof. B. Kozankiewicz
Institute of Physics, Polish Academy of Sciences
Al. Lotnikow 32/46, 02-668 Warsaw, Poland

Supporting information for this article is available on the WWW under https://doi.org/10.1002/cphc.202100679

decay from the triplet state to the singlet ground state will be reduced, enhancing the phosphorescence quantum yield.[25,26]

Over the years, the spectroscopy of single perylene molecules has been studied in the polymer polyethylene,[27] the Shpol'skii matrix *n*-nonane[28] and organic crystalline hosts such as biphenyl[22] and ortho-dichlorobenzene (*o*-DCB).[2] In almost all of the studied hosts, single-molecule emission of perylene was accompanied with spectral diffusion,[22] broadened linewidths,[22] or low fluorescence rate due to long dark times.[2] One way to increase a molecule's fluorescence rate is by recovering an emitter from its dark triplet state by exciting it with visible light of sufficient energy back to its excited singlet state – a phenomenon that is known as reverse intersystem crossing (rISC). Although rISC was first observed in 1969 by Keller,[29] it remains a scarcely studied effect at low temperature. To our knowledge, rISC has never been observed for lifetime-limited emitters below 5 K. A typical system that exhibits lifetime-limited emission below 5 K, namely terrylene in *p*-terphenyl,[30] had negligible effects of rISC below 30 K, however rISC became increasingly strong at temperatures above 50 K.[31,32] In non-lifetime-limited systems, and especially at room temperature, rISC is a much more common effect and was for example achieved by using a secondary laser beam that was red-shifted with respect to the probe beam to recover a molecule from the dark triplet state and to enhance the fluorescence signal.[33] However, this required much higher light intensities (from tens of $kWcm^{-2}$ up to several $MWcm^{-2}$, at an increased risk of photobleaching the molecule[33]) than typically used in cryogenic SMS (0.01–10 $W\,cm^{-2}$).[34] The rISC mechanism has also been utilized for improving the efficiency of organic light-emitting diodes.[35] While characterizing this new system of perylene-d12 in dibenzothiophene, we discovered that the brightness of single emitters in this system can be markedly increased and the triplet dark times significantly shortened with increasing intensity of the excitation beam. Importantly, we observed rISC mediated by the same beam that probes a single molecule. In this work, the power dependence of rISC was studied on a single perylene molecule by measuring the autocorrelations of its resonance fluorescence over a broad range of laser excitation intensities. We additionally provide an analytical framework to explain the experimental results by taking into account the process of rISC.

Experimental Section

Confocal Fluorescence Spectroscopy Setup

The samples were measured in a liquid helium flow cryostat (Janis, SVT-200-5) that can reach a working temperature of 1.3 K. With an objective (0.85 NA, Edmund Optics) immersed in liquid helium, the cryostat forms part of a home-built confocal microscope. A Ti:sapphire laser (M-squared SolsTiS) in combination with a frequency-doubling module (M-squared ECD-X) was used as a narrow bandwidth (<1 MHz) tunable excitation source, operating in the 440–460 nm range. The output wavelength of the laser was measured continuously with a wavemeter (High Finesse WS6-200), with resolution of a few MHz. A dichroic mirror (Semrock, FF458-Di02-25x36) was used to separate fluorescence from the excitation light and further filtering was done by a long-pass filter (Chroma, ET460lp). The laser beam was scanned over the sample by a scanning mirror (Newport, FSM-300-01) and fluorescence was detected by an avalanche photodiode (Excelitas, SPCM-AQRH-16). Fluorescence spectra were recorded with a Horiba iHR320 spectrometer coupled to a liquid-nitrogen-cooled Symphony II CCD detector. The excitation intensity was measured with a power meter (Newport 1830-C), before the laser beam entered the cryostat.

Preparation of Perylene-Doped Dibenzothiophene Crystals

Perylene-d12 (Sigma-Aldrich, 98%) was dissolved in toluene (Acros Organics, 99.85%) and diluted to concentrations of 10–100 ppm for bulk spectroscopy and 0.1–10 ppb for single-molecule spectroscopy measurements. The commercially obtained dibenzothiophene (Alfa Aesar, 98%) was heated above its melting point by a heat gun and a small quantity of the perylene in toluene solution was pipetted into the hot liquid.

For the bulk spectroscopy, square borosilicate capillaries (Vitro-Tubes, 1 mm ID and 0.2 mm walls) were filled with a molten solution of dibenzothiophene doped with perylene-d12. The capillaries were subsequently quenched in liquid nitrogen to rapidly crystallize and reduce the formation of perylene dimers producing excimer emission. Zone-refined dibenzothiophene was used for single-molecule spectroscopy experiments. The hot liquid solution of perylene-d12 in dibenzothiophene was allowed to crystallize and a few crystal grains were melted and pressed in between two glass slides, yielding a thin layer of organic material. Finally, the crystals were molten again and freeze-quenched in liquid nitrogen. All preparation steps were performed in normal atmosphere.

2. Results and Discussion

2.1. Line-Narrowing Spectroscopy

In this work, we have used for the first time dibenzothiophene (DBThio) as a host matrix for perylene-d12 (from now on simply referred to as perylene). DBThio is a sulphur-containing planar molecule forming a monoclinic unit cell with four molecules.[36] The origin of absorption of the singlet state is at 29923 cm^{-1} (334.3 nm) and phosphorescence is around 24292 cm^{-1} (411.8 nm).[37] Both the singlet and triplet of DBThio are higher in energy than the excited singlet state of perylene. The higher electronic energy levels of the host prevent intermolecular ISC, which is responsible for efficient quenching of single-molecule fluorescence of perylene in anthracene[22] and of terrylene in anthracene.[24]

At a temperature of 1.3 K, the excitation of the strongest vibronic line of perylene in DBThio at 447.2 nm shows line-narrowing of the 0–0 zero-phonon line (ZPL) in the bulk spectrum of a polycrystalline sample (Figure 1). The full-width-at-half-maximum (FWHM) of the inhomogeneous band of the 0–0 ZPL was measured by a narrow-range excitation spectrum around the strong 344 cm^{-1} vibronic line and was established to be 10 ± 1 cm^{-1}. The inhomogeneous broadening of the 0–0 ZPL and the vibronic lines in the bulk spectrum are comparable to those of perylene in other matrices.[22,27,28] The

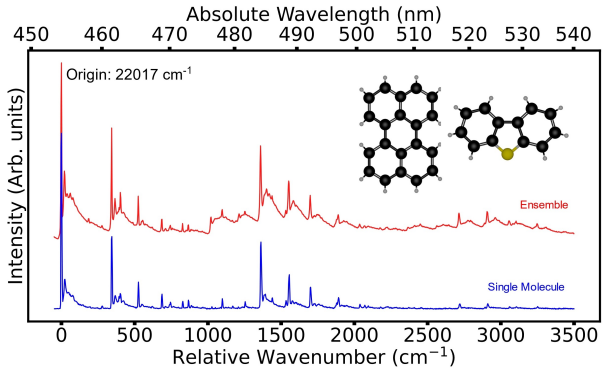

Figure 1. Fluorescence spectra of a single perylene molecule embedded in DBThio (blue) and of an ensemble of perylene molecules in a bulk polycrystalline sample (red). The bulk spectrum was obtained by exciting the strongest vibronic line around 447.2 nm and the single-molecule spectrum was made by excitation at 447.1 nm. The two strongest vibronic lines are shifted by 344 cm^{-1} and 1362 cm^{-1} with respect to the 0–0 ZPL, located at 22017 cm^{-1}. For peak positions see the Supporting Information S1. The molecular structures of perylene (left) and dibenzothiophene (right) are shown on the top right.

peak of the 0–0 ZPL lies around $22017 \pm 1.3\ cm^{-1}$ with no obvious other sites. From the emission spectrum of a single perylene molecule, the Debye-Waller factor, defined as the ratio of the 0–0 ZPL to the 0–0 phonon sideband, was determined to be approximately 0.40 ± 0.05. The assignments of the specific vibrational modes of perylene-h12[38,39] and perylene-d12 can be found elsewhere.[38–41]

2.2. Single-Molecule Fluorescence Spectroscopy

The phonon states in the crystal matrix are drastically depopulated at cryogenic temperatures and single molecules of perylene can be excited individually by their purely electronic transition to the singlet excited state – the 0–0 zero-phonon line. In order to find relatively isolated molecules in frequency space, the concentration and method of preparation had to be optimized. When the step of fast crystallization due to freeze-quenching was skipped, the perylene molecules tended to pack at the edges of the crystals and could not be distinguished spectrally (Supporting Information S2). Furthermore, the crystal thickness and concentration of perylene were of influence on the background signal and spectral diffusion. A dopant concentration of approximately 1 ppb was optimal for finding isolated molecular resonances.

The single-molecule fluorescence measurements we report on will relate to a single molecule (M1) that is representative for the perylene molecules in the DBThio matrix. In Figure 2, single-scan excitation spectra of perylene molecule M1 are shown at two different excitation intensities. Below the saturation intensity (Figure 2a) the molecule behaves typically as perylene in other systems, showing many events of ISC, which lead to reduced average fluorescence brightness.[2,22,27,28] Unique to this studied system is the behaviour at excitation intensities far above the saturation intensity (Figure 2b), where the fluorescence is much brighter and ISC seemingly has a negligible effect on the fluorescence rate. As the integration times are identical for both scans in Figure 2, we conclude that the effective lifetime of the triplet state is significantly shortened at high excitation intensities.

Molecule M1 has a homogeneous linewidth of 58 ± 1 MHz given by the FWHM of the Lorentzian curve fitted to the spectrum in Figure 3a. Typically, the perylene molecules in the DBThio matrix have homogeneous linewidths between 50 MHz and 70 MHz, which is comparable to the narrowest linewidths found for perylene in the *o*-DCB matrix.[2] All molecules appeared to show some degree of spectral diffusion, but for most molecules this was limited to diffusion within their linewidth on a timescale of minutes. This is also largely the case for molecule M1 (Figure 3b).

The spectral broadening of molecule M1 with the excitation intensity was quantified by fitting a Lorentzian curve to an averaged spectrum made out of multiple frequency linescans. Due to the ISC the individual scans appeared in stochastic shapes (Supporting Information S3) and produce a poor fit. Nevertheless, averaging multiple spectra may induce extra broadening of the linewidth due to spectral diffusion and/or small drifts of the laser. To check whether this was indeed the case, the lifetime of perylene-d12 in dibenzothiophene was measured to be 4.6 ± 0.1 ns (Supporting Information S5). The lifetime-limited linewidth is therefore around 35 ± 1 MHz and suggests that the homoge-

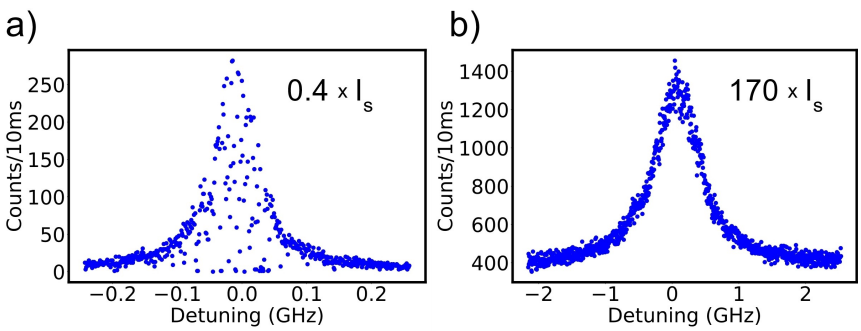

Figure 2. Single-scan fluorescence excitation spectra of single perylene molecule M1 taken at two excitation intensities, given in terms of the saturation intensity I_s. a) $0.4 \times I_s$ (b) $170 \times I_s$. The lines were scanned around a center wavelength of 454.57 nm, with an integration time of 10 ms per point.

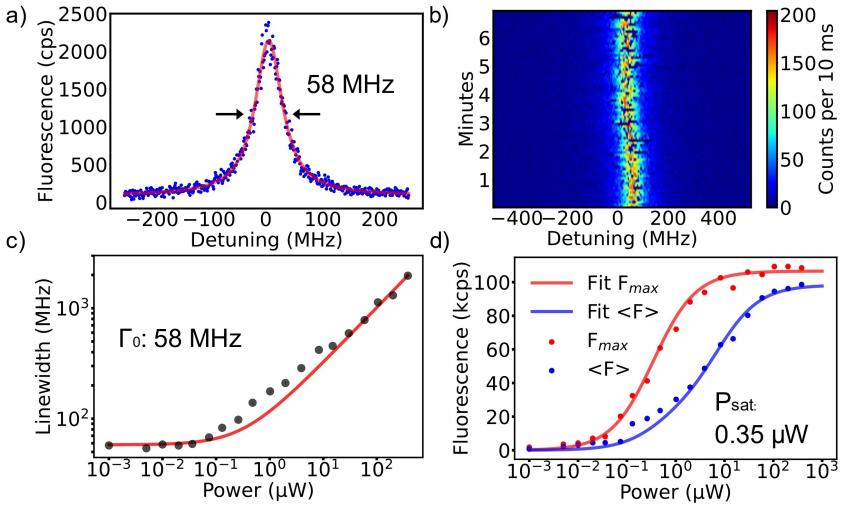

Figure 3. Spectral properties of molecule M1 at T = 1.3 K. a) Lorentzian fit to the average of 10 individual spectra taken at an excitation intensity of $0.02 \times I_s$. This fit points to a homogeneous linewidth of 58 MHz. The stochastic blinking in single traces is averaged out. b) The fluorescence signal is followed in real time by 84 single linescans. The color bar represents the fluorescence counts per 10 ms. c) Broadening of the linewidth of the molecule with excitation power. Deviations from the red curve at medium powers are likely caused by the spectral broadening due to averaging over multiple scans. d) Saturation behaviour of the molecule with excitation power. The red dots represent the *maximum* detected fluorescence, while the blue dots represent the *average* fluorescence rate. The red dots have been fitted with the red line according to equation 2 and the blue dots have been fitted with the blue line according to equation 3.

neous linewidth of 58 MHz is probably broadened by weak spectral diffusion and/or small drifts of the laser.

The spectral broadening of the molecule's linewidth as a function of excitation intensity was fitted using the standard formula:

$$\Gamma(I) = \Gamma_0 \sqrt{1 + \frac{I}{I_s}}. \quad (1)$$

The fit resulted again in a homogeneous linewidth Γ_0 of 58 ± 1 MHz and a saturation power P_{sat} of 0.35 ± 0.04 μW (Figure 3c). It should be noted that the laser power was measured before the laser beam entered the cryostat and is therefore not corrected for any power losses hereafter. Correcting for optical losses after the point of measurement and taking into account the spot size of the laser beam at the position of the molecule, found to have a FWHM of approximately 1 μm, we find an approximate saturation intensity I_s of 22 ± 3 W/cm^2.

The saturation of the fluorescence detected from the molecule was fitted in two ways (Figure 3d). The first fit (red points and red line in Figure 3d) was performed on the maximum resonance fluorescence signal we detected from the molecule. We assume that this maximum originates from time intervals where the molecule practically skips the triplet level while cycling through the singlet ground and excited state. This fits to a standard sigmoid-shaped saturation curve given by:

$$F(I) = F_\infty \frac{I/I_s}{1 + I/I_s}. \quad (2)$$

This fit gave us a fluorescence detection limit at full saturation of approximately 106 kcps. We note that this is comparable to bright emitters studied in our cryogenic microscope, which has a relatively low collection efficiency due to a lack of immersion.

Although for short periods the fluorescence detected from a molecule can reach the saturation limit of the red line in Figure 3d, the average fluorescence limit $\langle F(\infty) \rangle$ will be at a lower level due to frequent interruptions of the singlet Rabi cycle while the molecule is in the dark triplet state. The average fluorescence detected from the molecule is given by the blue points in Figure 3d. Normally, the fluorescence intensity would saturate in the same sigmoid-shape as the red curve, but the blue points clearly follow a pattern that diverges from it. At high excitation intensities the average fluorescence intensity tends to converge to the limit where the triplet state plays a negligible role on the fluorescence yield. To explain this deviation from the standard saturation model we propose a four-level scheme including rISC.

The relevant intramolecular rates of the commonly used level scheme are shown in Figure 4. The rate k_{12} is the population rate of the singlet excited state and depends on the excitation intensity, while k_{21} is the depopulation rate of the singlet excited state. The symbols k_{23}^{xy} and k_{23}^{z} are the *effective* ISC rates towards the T_{xy} and T_z triplet states and γ_{31}^{xy} and γ_{31}^{z} are the two triplet states' depopulation rates. We were able to fit the experimental data in Figure 3d (blue points) by including a rISC term that is linearly dependent on the optical intensity. According to Ambrose et al.[42,43] the saturation of a three-level system in terms of all the intramolecular rates shown in Figure 4 is given by:

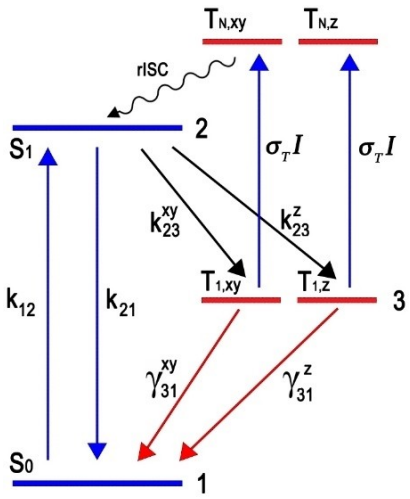

Figure 4. Jablonski diagram of the four-level system of perylene, with S_0 and S_1 being the singlet ground and excited state, and T_{xy} and T_z being two distinguishable intermediate states out of the three-sublevel manifold, referred to as "the triplet state". A most likely pathway for rISC is shown here as an absorption of a photon that excites the molecule from the T_1 state to a higher excited triplet state T_N at a rate $\sigma_T I$ proportional to the intensity (σ_T being the absorption cross section of the triplet states). From the higher excited triplet state a spin-forbidden transition to the singlet manifold completes the cycle. The whole process is referred to as rISC and occurs at a rate αI proportional to the excitation intensity.

$$F(I) = \eta \frac{\Phi_F \tau_F^{-1}}{2 + {k_{23}^{xy}}/{\gamma_{31}^{xy}} + {k_{23}^{z}}/{\gamma_{31}^{z}}} \frac{{I}/{I_s}}{1 + {I}/{I_s}}, \quad (3)$$

with η our setup-dependent detection efficiency and Φ_F the radiative quantum yield of the $S_1 \rightarrow S_0$ transition of perylene. Lastly, the quantity τ_F is the fluorescence lifetime, which was determined to be 4.6 ± 0.1 ns.

To include rISC, we introduce the *effective* triplet depopulation rates, which are parametrized to be linearly dependent on the excitation intensity as:

$$k_{31}^{xy}(I) = \gamma_{31}^{xy} + \alpha I, \; k_{31}^{z}(I) = \gamma_{31}^{z} + \alpha I \quad (4)$$

Here, we assumed that the lifetimes of the higher excited triplet states $T_{N,xy}$ and $T_{N,z}$ are very short, so that transitions from the triplet state(s) to the singlet manifold occur at an effective rate αI proportional to the laser intensity. As we will show in the next section, we derived the ISC rate, lifetime of the triplet states γ_{31}^{xy} and γ_{31}^{z} and the rISC parameter α by a model based on fluorescence correlation functions that was processed in a global fit, together with equation 1 and 2. As our data do not allow us to distinguish a possible difference between the laser-induced rISC rates of the two effective triplet sublevels, we assumed them to be equal (see further discussion in sec. 3.3). Equation 4 was substituted into equation 3 to include rISC and was added to the global fit to find the values of the common parameters that fitted best to the experimental data. The global fit resulted in the blue line to the blue points in Figure 3d. The detection efficiency η multiplied by the quantum yield Φ_F was determined to be 9×10^{-4}, which is a typical value for our setup when assuming Φ_F to be close to unity.[44] The low detection yield is likely due to the lower quantum efficiency of our detector at shorter wavelengths and the additional losses of our cryogenic confocal setup, which is optimized for near IR. The saturated average fluorescence rate found in the blue curve of Figure 3d (100 kcps) is at least fourfold higher than it would be in the absence of rISC (22 kcps), i.e. when α is taken to be zero.

2.3. A Model for ISC with rISC

ISC dynamics were studied in detail by capturing resonance fluorescence time traces. Time trace data from a single APD was gathered over the course of 30 s up to 3 minutes with an integration time of 10 µs. Subsequently, the time trace data served as input for the calculation of the correlation function $g^{(2)}(\tau)$ by using the formula:

$$g^{(2)}(\tau) = \frac{\langle I(t) I(t+\tau) \rangle}{\langle I(t) \rangle^2}. \quad (5)$$

The autocorrelations were obtained at a broad range of excitation intensities, in order to observe if there was any saturation of the correlation time and of the correlation contrast at high intensities, as is common for regular ISC.[2] However, this was not the case. Instead, the dark times become shorter with higher excitation power as can be noted from the time traces shown in Figure 5.

At low excitation intensities a clear distinction can be made between a short exponential decay and a longer exponential decay (Figure 5a). The short decay is usually attributed to the indistinguishable T_{xy}-states and the longer decay to the T_z-state.[45] As the laser intensity increases, the two exponential decays move closer to each other, up to the point where a single exponential fit, as given by the first two terms of equation 6, matches the best with the experimental data. Hence, there seems to be no selectivity of rISC for the two distinguishable triplet states and at higher intensities the lifetimes of the levels appear to converge to the same time regimes. In particular, our analysis of power-dependent autocorrelation curves suggest that the T_z-state seems to be affected sooner by rISC than the shorter-lived T_{xy}-state. The reasoning behind this is, that the longer lifetime increases the chance of inducing rISC with the probe beam. The quick disappearance of the second exponent from the autocorrelation curves, while the excitation intensity increases, limits the number of data points that can be obtained for the T_z-state.

For low excitation intensities ($< I_s$) the autocorrelations were fitted to a bi-exponential model function of the form:

$$g^{(2)}(\tau) = C_0 + C_1 e^{-\lambda_1 \tau} + C_2 e^{-\lambda_2 \tau}. \quad (6)$$

C_0 was generally close to 1, but can deviate from it due to stray correlations. To correct for stray correlations the contrasts C_1 and C_2 of the exponentials were divided by C_0. Other periodical stray correlations originating from vibrations coupling to our cryostat were removed by dividing $g^{(2)}(\tau)$ by a

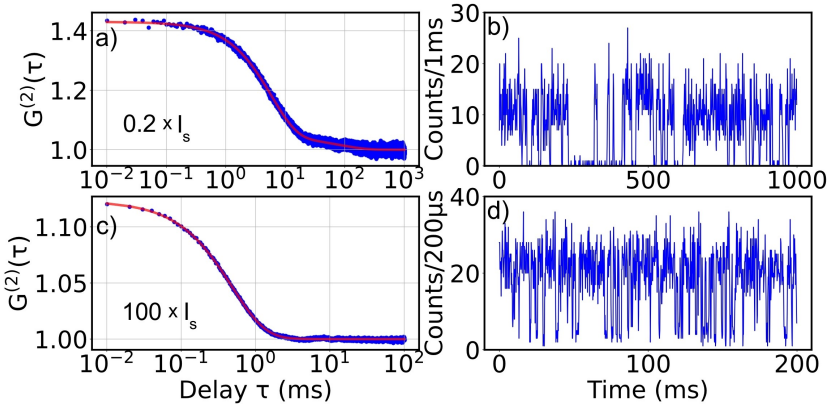

Figure 5. Fitted autocorrelation curves (left) and parts of the corresponding fluorescence time traces (right) of molecule M1 recorded at two excitation intensities, namely a) and b) at $0.2 \times I_s$, c) and d) at $100 \times I_s$. Note that in d) the number of dark periods is larger for high excitation intensities due to saturation, however their durations are much shorter. The correlation function in a) is fitted to a bi-exponential decay (equation 6) and the correlation function in c) is fitted to a single exponential decay (first two terms of equation 6).

normalized correlation of the background signal (Supporting Information S4). Lastly, the contrasts are also corrected for background counts consisting mostly of dark counts and leakage through the filter due to scattering at higher laser intensities. The prefactor $(1 + B/S)^2$ corrects for the strength of the background B with respect to the fluorescence signal S from the molecule.[46] The signal and background were extracted from single-molecule excitation spectra measured at equal intensities and the background never exceeded more than 40% of the signal from the molecule. At high excitation intensities ($> I_s$) we fitted the correlation curves to a single exponential, which is given by the first two terms of equation 6 and the same corrections were performed. More details on the measurements of fluorescence time traces can be found in the Supporting Information Section S4.

Using the model, explained in detail in references,[2,45] we related the contrasts C_1 and C_2 and the decay parameters λ_1 and λ_2 to the *effective* ISC rates (k_{23}^{xy}, k_{23}^{z}) and the *effective* triplet depopulation rates (k_{31}^{xy}, k_{31}^{z}). The reader is referred to Supporting Information Section S6 for a complete derivation of the model. The *effective* ISC rates are directly related to the degree of saturation of the molecule and reach a maximum when the molecule reaches the highest probability of populating the singlet excited state. The relation of the *effective* ISC rates to the saturation of the molecule is given by:

$$\left(k_{23}^{xy},\ k_{23}^{z}\right) = \frac{\left(\gamma_{23}^{xy}, \gamma_{23}^{z}\right)}{2} \frac{I/I_s}{1 + I/I_s}. \tag{7}$$

Through inspection of the series of time traces and their respective autocorrelations as functions of excitation intensity, such as the ones presented in Figure 5, we conclude that the time spent in the triplet state is significantly reduced at higher excitation intensities. The *intrinsic* triplet depopulation rates, related to the lifetime of the triplet states, were therefore modelled to be linearly dependent on excitation intensity as in equation 4, referred to as the *effective* triplet depopulation rates. In this way rISC provides an additional channel for depopulating the triplet state.

The contrasts C_1 and C_2 are related to the *effective* rates of ISC (k_{23}^{xy}, k_{23}^{z}) and *effective* triplet depopulation rates (k_{31}^{xy}, k_{31}^{z}) by:

$$C_{1,2} = \frac{\lambda_{2,1}\left(k_{31}^{xy} - \lambda_{1,2}\right)\left(k_{31}^{z} - \lambda_{1,2}\right)}{k_{31}^{xy} k_{31}^{z}\left(\lambda_{1,2} - \lambda_{2,1}\right)}, \tag{8}$$

where the decay parameters λ_1 and λ_2 are given by:

$$\lambda_{1,2} = \frac{1}{2}(\Sigma \pm D), \tag{9}$$

with Σ the sum of all rates and D the discriminant of the characteristic equation (Supporting Information S6), both given by:

$$\Sigma = k_{23}^{xy} + k_{23}^{z} + k_{31}^{xy} + k_{31}^{z}, \tag{10}$$

$$D = \sqrt{\Sigma^2 - 4\left(k_{23}^{xy} k_{31}^{z} + k_{23}^{z} k_{31}^{xy} + k_{31}^{xy} k_{31}^{z}\right)}. \tag{11}$$

Figure 6 depicts the values found for the contrasts C_1 and C_2 and decay parameters λ_1 and λ_2. Because of the dependence of k_{23}^{xy} and k_{23}^{z} on the level of saturation (equation 7) and the proportionality of C_1 to k_{23}^{xy} and C_2 to k_{23}^{z}, the contrasts are expected to saturate as a sigmoidal curve. However, due to rISC the contrasts C_1 and C_2 also decrease as $(\alpha I)^{-1}$. This leads to a decreasing contrast at high excitation intensities, as was observed for the contrast C_1 in Figure 6a. The contrast of C_2 is already low before saturation and decreases quickly due to this proportionality to $(\alpha I)^{-1}$. The limited number of points for C_2 makes it impossible to detect a difference in rISC efficiency. Indeed, optical excitation of the substates of the lowest triplet level to a highly excited triplet state is not spin-selective. If this excitation is the rate-limiting step, i.e., if further relaxation back

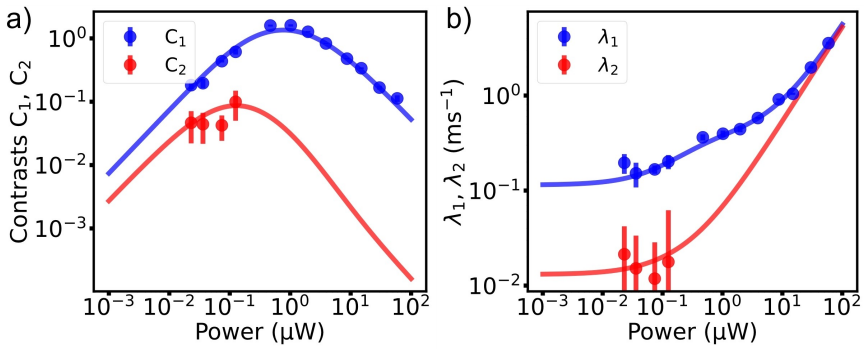

Figure 6. a) Contrast values and b) decay strength values plotted as functions of excitation power. The blue and red points are obtained from the fits to autocorrelation curves and the contrasts are corrected for background and stray correlations. The blue and red lines represent an error-weighted global fit to the data points.

to the singlet space is much faster, the resulting rISC rate would not be spin-dependent. In this case, therefore, we expect the same rISC rates for all three triplet sublevels.

The values found for the contrasts C_1 and C_2 and decay parameters λ_1 and λ_2 at different excitation intensities were part of the global fit to find the optimal values for γ_{23}^{xy}, γ_{23}^{z}, γ_{31}^{xy}, γ_{31}^{z} and α. The fit was logarithmically-weighted with the errors obtained from the individual fits to the correlation curves.

For molecule M1 the *intrinsic* triplet lifetimes $(\gamma_{31}^{xy})^{-1}$ and $(\gamma_{31}^{z})^{-1}$ were respectively determined to be 8.8 ± 0.6 ms and 77 ± 10 ms. The rISC parameter α varies between molecule M1-M3, but normalized for the saturation intensity I_s, they are similar in size. The average triplet lifetimes of the global fits for molecule M1–M3 yield a triplet lifetime of the T_{xy}-state ($\langle\gamma_{31}^{xy}\rangle^{-1}$) of 8.5 ± 0.4 ms and 64 ± 12 ms for the T_z-state ($\langle\gamma_{31}^{z}\rangle^{-1}$). The average ISC rates are $531\pm26\ s^{-1}$ for $\langle\gamma_{23}^{xy}\rangle$ and $46\pm19\ s^{-1}$ for $\langle\gamma_{23}^{z}\rangle$. The large uncertainty in the *intrinsic* triplet depopulation rates γ_{31} for the molecules reported in Table 1 arises from the low photon counts of the measurements at low power. At higher power, these rates are dominated by the rISC parameter α (see Equation 4). Furthermore, the heterogeneity of embedding sites and defects in the polycrystalline samples may contribute to the variability of the measured parameters.

The lifetimes of the two triplet states are longer than reported for perylene in *o*-DCB[2] (3.0 ms and 19 ms) and *n*-nonane[28] (1.1 ± 0.5 ms), which might be related to the deuteration of the perylene.[26] In general the triplet lifetimes are reported to be longer for deuterated fluorophores compared to their non-deuterated analogues.[26] For perylene-d12 dissolved in PMMA, the triplet lifetime was found to increase by a factor of 2.3 (298 K) compared to perylene-h12.[26] The triplet yield $\phi_T = \tau_F\left(k_{23}^{xy} + k_{23}^{z}\right)$ was determined to be on the order of 3×10^{-6}, which is comparable to the triplet yield found for perylene-h12 in *o*-DCB.[2]

The reason for efficient rISC taking place in this particular matrix, as opposed to other matrices that have been used for perylene, remains unknown. Assuming that the excitation beam excites the triplet state to a higher triplet level there are at least two pathways for the rISC. The most commonly proposed pathway involves an intramolecular intersystem crossing, i.e., a spin-flip process when the perylene molecule is in a high triplet level.[33,35] The high density of vibrational states in both multiplicities makes it easy to achieve resonance between triplet and singlet levels, leading to relaxation to the lower singlet states. The large T_1-T_N energy gap and energetic proximity of T_N and S_N states can favour rISC over an internal conversion process from T_N to T_1.[35] The relatively heavy sulphur atom of the DBThio matrix could further help couple singlet and triplet states, particularly in the more delocalized orbitals of the higher excited states.[47] If this triplet-to-singlet transition is fast enough, the rISC rate would be dominated by the optical excitation of the T_{xy} and T_z states, leading to the same rISC rate for all three triplet sublevels. A less-likely pathway for rISC could involve a Dexter exchange with the host's triplet state, producing a triplet excitation of a neighbor DBThio molecule by Dexter energy transfer. However, this excitation might again relax by another Dexter process to the perylene triplet, bringing the perylene molecule back to the triplet multiplicity. Lastly, the efficiency of rISC does not appear to vary significantly from molecule to molecule. However, the rISC process could be of use while doing spectroscopic studies on the excited triplet states by not using the optical fluorescence-exciting beam to induce rISC, but by using a secondary tunable beam[33] or a time-gated double excitation method to determine the quantum yields of the T_N to S_1 rISC.[47] The rISC process might also be harnessed for a better control of triplet blinking in view of fluorescence superresolution STORM schemes at low temperature.[5,48,49]

Table 1. Reported results of the global fit for three individual molecules, for parameters as described in the main text and Figure 4. The reported errors are standard deviations obtained from the global fit.

	γ_{23}^{xy} (s^{-1})	γ_{31}^{xy}(s^{-1})	γ_{23}^{z}(s^{-1})	γ_{31}^{z}(s^{-1})	$\alpha(\mu W^{-1}s^{-1})$
M1	542 ± 25	114 ± 9	23 ± 6	13 ± 2	52.3 ± 0.8
M2	550 ± 70	91 ± 7	76 ± 55	15 ± 11	14.2 ± 0.6
M3	500 ± 27	146 ± 11	38 ± 13	19 ± 3	26.5 ± 0.9
	I_s[Wcm^{-2}]	F_∞[kcps]		Γ_0[MHz]	λ0−0 ZPL [nm]
M1	22 ± 3	106 ± 1		58 ± 1	454.57
M2	82 ± 20	51 ± 5		55 ± 2	454.38
M3	59 ± 5	155 ± 2		59 ± 1	454.36

3. Conclusion

Deuterated perylene in dibenzothiophene is not the most spectrally stable system. However, the fluorescence we detected from a single perylene molecule is on par with other bright systems commonly employed as lifetime-limited single-molecule emitters. That is a direct consequence of rISC that allows the recovery of the molecule from the perylene's long-lived triplet state and at least quadruples the detectable fluorescence rate. By studying the autocorrelations of resonance fluorescence time traces we were able to estimate the intrinsic triplet lifetimes of deuterated perylene to be 8.5 ± 0.4 ms for the T_{xy}-state and 64 ± 12 ms for the T_z-state. In addition, we were able to quantify the effect of rISC on the depopulation rate of the triplet states. The demonstrated effect of rISC could be used in the future quantum studies of triplet-state manipulation of single emitters, for superresolution at cryogenic temperatures, for enhancing the fluorescence emission, and for recovering single emitters from long-lived triplet states.

Acknowledgements

We would like to thank Dr. Amin Moradi for his help with the optical setup and Ms Maialen Ortego Larrazabal for her help with bulk spectroscopy measurements. Finally, we thank Dr. Olaf Morawski for his help with the setup for TCSPC.

Conflict of Interest

The authors declare no conflict of interest.

Keywords: single-molecule spectroscopy · triplet states · reverse intersystem crossing · fluorescence blinking · intrinsic lifetimes

[1] T. Basché, S. Kummer, C. Bräuchle, *Nature* **1995**, *373*, 132–134.
[2] N. R. Verhart, P. Navarro, S. Faez, M. Orrit, *Phys. Chem. Chem. Phys.* **2016**, *18*, 17655–17659.
[3] A. A. L. Nicolet, C. Hofmann, M. A. Kol'chenko, B. Kozankiewicz, M. Orrit, *ChemPhysChem* **2007**, *8*, 1215–1220.
[4] C. Toninelli, I. Gerhardt, A. S. Clark, A. Reserbat-Plantey, S. Götzinger, Z. Ristanović, M. Colautti, P. Lombardi, K. D. Major, I. Deperasińska, W. H. Pernice, F. H. L. Koppens, B. Kozankiewicz, A. Gourdon, V. Sandoghdar, M. Orrit, *Nat. Mater.* **2021**, DOI: 10.1038/s41563-021-00987-4.
[5] D. P. Hoffman, G. Shtengel, C. S. Xu, K. R. Campbell, M. Freeman, L. Wang, D. E. Milkie, H. A. Pasolli, N. Iyer, J. A. Bogovic, D. R. Stabley, A. Shirinifard, S. Pang, D. Peale, K. Schaefer, W. Pomp, C.-L. Chang, J. Lippincott-Schwartz, T. Kirchhausen, D. J. Solecki, E. Betzig, H. F. Hess, *Science* **2020**, *367*, DOI: 10.1126/science.aaz5357.
[6] S. Weisenburger, B. Jing, D. Hänni, L. Reymond, B. Schuler, A. Renn, V. Sandoghdar, *ChemPhysChem* **2014**, *15*, 763–770.
[7] S. Weisenburger, D. Boening, B. Schomburg, K. Giller, S. Becker, C. Griesinger, V. Sandoghdar, *Nat. Methods* **2017**, *14*, 141–144.
[8] W. Li, S. C. Stein, I. Gregor, J. Enderlein, *Opt. Express* **2015**, *23*, 3770.
[9] P. D. Dahlberg, A. M. Sartor, J. Wang, S. Saurabh, L. Shapiro, W. E. Moerner, *J. Am. Chem. Soc.* **2018**, *140*, 12310–12313.
[10] A. Moradi, Z. Ristanović, M. Orrit, I. Deperasińska, B. Kozankiewicz, *ChemPhysChem* **2019**, *20*, 55–61.
[11] M. Colautti, F. S. Piccioli, Z. Ristanović, P. Lombardi, A. Moradi, S. Adhikari, I. Deperasinska, B. Kozankiewicz, M. Orrit, C. Toninelli, *ACS Nano* **2020**, *14*, 13584–13592.
[12] A. Shkarin, D. Rattenbacher, J. Renger, S. Hönl, T. Utikal, P. Seidler, S. Götzinger, V. Sandoghdar, *Phys. Rev. Lett.* **2021**, *126*, 133602.
[13] Y. Tian, P. Navarro, M. Orrit, *Phys. Rev. Lett.* **2014**, *113*, 135505.
[14] M. Rezai, J. Wrachtrup, I. Gerhardt, *Phys. Rev. X* **2018**, *8*, 031026.
[15] J. Hwang, M. Pototschnig, R. Lettow, G. Zumofen, A. Renn, S. Götzinger, V. Sandoghdar, *Nature* **2009**, *460*, 76–80.
[16] S. Pazzagli, P. Lombardi, D. Martella, M. Colautti, B. Tiribilli, F. S. Cataliotti, C. Toninelli, *ACS Nano* **2018**, *12*, 4295–4303.
[17] R. C. Schofield, K. D. Major, S. Grandi, S. Boissier, E. A. Hinds, A. S. Clark, *J. Phys. Commun.* **2018**, *2*, 115027.
[18] D. Wang, H. Kelkar, D. Martin-Cano, D. Rattenbacher, A. Shkarin, T. Utikal, S. Götzinger, V. Sandoghdar, *Nat. Phys.* **2019**, *15*, 483–489.
[19] J. Wrachtrup, C. von Borczyskowski, J. Bernard, M. Orrit, R. Brown, *Nature* **1993**, *363*, 244–245.
[20] M. Orrit, *Nature* **2009**, *460*, 42–44.
[21] P. Navarro Perez, *PhD Thesis: Stable Single Molecules for Quantum Optics and All-Optical Switches*, Leiden University, **2014**.
[22] P. J. Walla, F. Jelezko, P. Tamarat, B. Lounis, M. Orrit, *Chem. Phys.* **1998**, *233*, 117–125.
[23] R. H. Clarke, R. M. Hochstrasser, *J. Mol. Spectrosc.* **1969**, *32*, 309–319.
[24] A. Nicolet, M. A. Kol'chenko, B. Kozankiewicz, M. Orrit, *J. Chem. Phys.* **2006**, *124*, 164711.
[25] W. Siebrand, *J. Chem. Phys.* **1967**, *47*, 2411–2422.
[26] R. E. Kellogg, N. C. Wyeth, *J. Chem. Phys.* **1966**, *45*, 3156–3158.
[27] T. Basché, W. E. Moerner, *Nature* **1992**, *355*, 335–337.
[28] M. Pirotta, A. Renn, M. H. V. Werts, U. P. Wild, *Chem. Phys. Lett.* **1996**, *250*, 576–582.
[29] R. A. Keller, *Chem. Phys. Lett.* **1969**, *3*, 27–29.
[30] S. Kummer, Th. Basché, C. Bräuchle, *Chem. Phys. Lett.* **1994**, *229*, 309–316.
[31] M. Banasiewicz, O. Morawski, D. Wiącek, B. Kozankiewicz, *Chem. Phys. Lett.* **2005**, *414*, 374–377.
[32] L. Fleury, J.-M. Segura, G. Zumofen, B. Hecht, U. P. Wild, *Phys. Rev. Lett.* **2000**, *84*, 1148–1151.
[33] C. Ringemann, A. Schönle, A. Giske, C. von Middendorff, S. W. Hell, C. Eggeling, *ChemPhysChem* **2008**, *9*, 612–624.
[34] T. Plakhotnik, W. E. Moerner, V. Palm, U. P. Wild, *Opt. Commun.* **1995**, *114*, 83–88.
[35] D. Hu, L. Yao, B. Yang, Y. Ma, *Philos. Transact. A Math. Phys. Eng. Sci.* **2015**, *373*, 20140318.
[36] W. Goldacker, D. Schweitzer, H. Zimmermann, *Chem. Phys.* **1979**, *36*, 15–26.
[37] A. Bree, R. Zwarich, *Spectrochim. Acta Part Mol. Spectrosc.* **1971**, *27*, 621–630.
[38] I. I. Abram, R. A. Auerbach, R. R. Birge, B. E. Kohler, J. M. Stevenson, *J. Chem. Phys.* **1975**, *63*, 2473–2478.
[39] P. J. Unwin, T. S. Jones, *Surf. Sci.* **2003**, *532*, 1011–1016.
[40] Y. Suganuma, Y. Kowaka, N. Ashizawa, N. Nakayama, H. Goto, T. Ishimoto, U. Nagashima, T. Ueda, T. Yamanaka, N. Nishi, M. Baba, *Mol. Phys.* **2011**, *109*, 1831–1840.
[41] M. Sulkes, *Chem. Phys.* **1987**, *114*, 289–294.
[42] W. P. Ambrose, Th. Basché, W. E. Moerner, *J. Chem. Phys.* **1991**, *95*, 7150–7163.
[43] H. de Vries, D. A. Wiersma, *J. Chem. Phys.* **1980**, *72*, 1851–1863.
[44] M. Sonnenschein, A. Amirav, J. Jortner, *J. Phys. Chem.* **1984**, *88*, 4214–4218.
[45] A.-M. Boiron, B. Lounis, M. Orrit, *J. Chem. Phys.* **1996**, *105*, 3969–3974.
[46] J. Bernard, L. Fleury, H. Talon, M. Orrit, *J. Chem. Phys.* **1993**, *98*, 850–859.
[47] S. Kobayashi, K. Kikuchi, H. Kokubun, *Chem. Phys.* **1978**, *27*, 399–407.
[48] P. D. Dahlberg, W. E. Moerner, *Annu. Rev. Phys. Chem.* **2021**, *72*, 253–278.
[49] C. N. Hulleman, W. Li, I. Gregor, B. Rieger, J. Enderlein, *ChemPhysChem* **2018**, *19*, 1774–1780.

Manuscript received: September 15, 2021
Revised manuscript received: November 5, 2021
Accepted manuscript online: November 15, 2021
Version of record online: November 23, 2021